Radiology

Hidetake Yabuuchi, MD
Tatsuro Fukuya, MD
Tsuyoshi Tajima, MD
Yoichi Hachitanda, MD
Kichinobu Tomita, MD
Mitsuru Koga, MD

Index terms:
Magnetic resonance (MR), contrast enhancement, 264.121411, 264.121416, 264.12143
Salivary glands, MR, 264.121411, 264.121416, 264.12143
Salivary glands, neoplasms, 264.343, 264.363, 264.373

Published online before print
10.1148/radiol.2262011486
Radiology 2003; 226:345–354

Abbreviations:
ER = enhancement ratio
TIC = time–signal intensity curve
T_{peak} = time of peak enhancement
WR = washout ratio

[1] From the Departments of Radiology (H.Y., T.F., T.T., M.K.), Pathology (Y.H.), and Head and Neck Surgery (K.T.), National Kyushu Cancer Center, 3-1-1 Notame, Minami-ku, Fukuoka 811-1395, Japan. From the 2000 RSNA scientific assembly. Received September 5, 2001; revision requested October 16; final revision received July 10, 2002; accepted July 31. **Address correspondence to** H.Y. (e-mail: *hyabuu@nk-cc.go.jp*).

Author contributions:
Guarantor of integrity of entire study, H.Y.; study concepts and design, H.Y.; literature research, H.Y.; clinical studies, H.Y., T.F., T.T.; data acquisition, H.Y.; data analysis/interpretation, H.Y., T.F.; statistical analysis, H.Y.; manuscript preparation and definition of intellectual content, H.Y.; manuscript editing, T.F.; manuscript revision/review, T.F., Y.H., K.T.; manuscript final version approval, all authors.

Salivary Gland Tumors: Diagnostic Value of Gadolinium-enhanced Dynamic MR Imaging with Histopathologic Correlation[1]

PURPOSE: To evaluate the diagnostic value of gadolinium-enhanced dynamic magnetic resonance (MR) imaging of salivary gland tumors and correlate the MR imaging and histopathologic findings.

MATERIALS AND METHODS: Thirty-three salivary gland tumors in 29 patients were examined preoperatively at gadolinium-enhanced dynamic MR imaging. There were 22 benign and 11 malignant tumors. Dynamic contrast material–enhanced MR images were obtained for 5 minutes. Time of peak enhancement (T_{peak}) and washout ratio (WR) were determined from time–signal intensity curves (TICs). Microvessel count and cellularity-stromal grade were evaluated histopathologically. The strengths of correlations between T_{peak} and microvessel count and between WR and cellularity-stromal grade were statistically analyzed to determine whether any differences among the various histopathologic tumor types existed. In a validation study, 13 salivary gland tumors in 13 patients were examined consecutively.

RESULTS: At a T_{peak} of 120 seconds, malignant tumors could be differentiated from pleomorphic adenomas but not from Warthin tumors. A WR of 30%, however, enabled differentiation between malignant and Warthin tumors. Classification of TICs on the basis of a T_{peak} of 120 seconds and a WR of 30% had high sensitivity (91%) and specificity (91%) in the differentiation of benign and malignant tumors. Correlations between T_{peak} and microvessel count ($P < .0001$, $\rho = -0.800$) and between WR and cellularity-stromal grade ($P = .0105$, $\rho = 0.572$) were significant. The validation study also yielded high sensitivity (100%) and specificity (80%) in the differentiation between benign and malignant tumors.

CONCLUSION: Gadolinium-enhanced dynamic MR imaging is useful for differentiating benign from malignant salivary gland tumors.

It is clinically important to determine whether a salivary gland tumor is benign or malignant preoperatively, because this information strongly influences the surgical procedure. Local excision or superficial parotidectomy is performed to treat benign tumors, whereas total parotidectomy with or without removal of facial nerve tissue is performed to treat malignant tumors (1–4). Aggressive resection of any tumor, whether the neoplasm is benign or malignant, can cause serious complications such as facial nerve palsy, and surgeons use the more aggressive approach when they perform surgery to treat malignant tumors (1–4). Furthermore, preoperative aspiration cytology results are not always conclusive because insufficient specimens are sometimes obtained owing to a small sample size or the deep location of the tumor (5–7). Therefore, preoperative imaging has an important role in surgical planning.

The magnetic resonance (MR) imaging findings of salivary gland tumors have been described in a number of reports (8–15). It has been reported that the findings of low signal

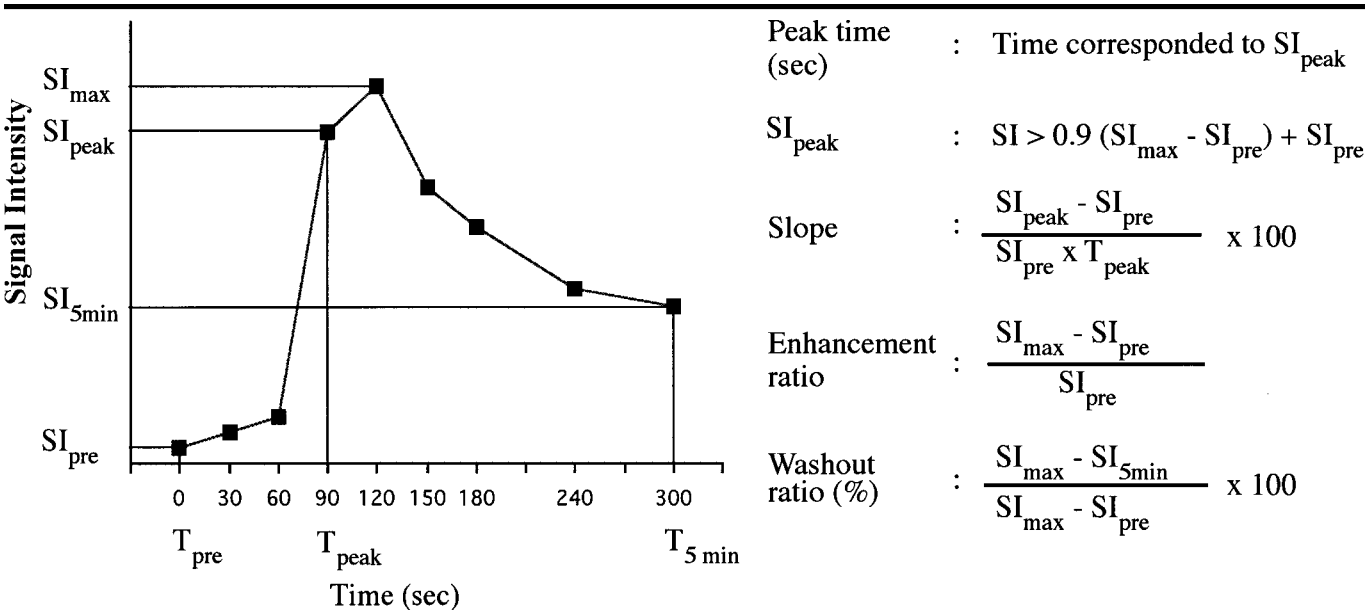

Figure 1. TIC constructed at dynamic gadolinium-enhanced MR imaging (left) and TIC parameter definitions (right).

intensity and irregular lesion margins on T2-weighted MR images indicate malignancy (8,9). However, the reported sensitivities and specificities of these findings have been low and significantly overlapping (10–12,15). The time of peak enhancement (T_{peak}) at dynamic MR imaging has been reported to have little diagnostic value in the differentiation between benign and malignant salivary gland tumors (16). One report (17) described gradual enhancement of both pleomorphic adenoma and adenoid cystic carcinoma at dynamic MR imaging. To our knowledge, however, there have been no studies of dynamic MR imaging of salivary gland tumors that were focused on any parameter of the time–signal intensity curve (TIC) except the T_{peak}. Also, to our knowledge, the relationship between TIC parameters and histopathologic findings has not been studied. The purpose of our study was to evaluate the diagnostic value of gadolinium-enhanced dynamic MR imaging of salivary gland tumors and the relationship between the dynamic MR imaging and histopathologic findings.

TABLE 1
Histopathologic Diagnoses of Salivary Gland Tumors

Diagnosis	No. of Lesions	
	Initial Study (n = 33)	Validation Study (n = 13)
Benign	22	10
Pleomorphic adenoma	12	5
Warthin tumor	9	4
Myoepithelioma	1	0
Eosinophilic granuloma	0	1
Malignant	11	3
Mucoepidermoid carcinoma	5	0
Adenoid cystic carcinoma	1	2
Adenocarcinoma	2	1
Non-Hodgkin lymphoma	2	0
Carcinoma in pleomorphic adenoma	1	0

MATERIALS AND METHODS

Patients and Salivary Gland Tumors

Between July 1998 and June 2000, we performed gadolinium-enhanced (gadopentetate dimeglumine, Magnevist; Nihon Shering, Osaka, Japan) dynamic MR imaging of a total of 40 lesions (in 36 patients) that were clinically suspected of being salivary gland tumors. The study protocol was approved by our institutional review board. All patients gave written informed consent to be imaged in the study. Seven lesions (in seven patients) were excluded from this study because they were proven to be inflammatory on the basis of a reduction in size after antibiotic therapy in three patients, an extrasalivary location at MR imaging in three patients, and the presence of chronic sialoadenitis, which was proven at surgery, in one patient. The remaining 33 salivary gland tumors in 29 patients (16 women, 13 men; age range, 27–77 years; mean age, 59 years) were included in this study. The tumor locations were as follows: 25 lesions in the parotid gland, five in the minor salivary gland, and three in the submandibular gland.

Histopathologic diagnoses were made on the basis of findings in specimens obtained at surgical resection of all lesions. The distributions of benign and malignant tumors are shown in Table 1. To compare the maximum tumor diameter between the benign and malignant neoplasms, we used an average and performed a per-person rather than per-tumor analysis to avoid a lack of independence, because our study included two mucoepidermoid carcinomas in one patient, two acinic cell carcinomas in one patient, and three Warthin tumors in one patient. The maximum diameter of the tumors ranged from 10 to 55 mm (mean, 25.8 mm). The mean maximum diameter of the benign

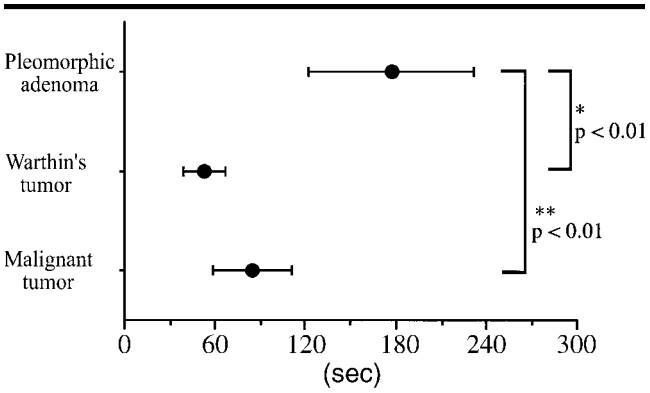

Figure 2. Plotted T_{peak} values. The dots represent means, and the lines through the dots represent SDs. * = *P* value for comparison of pleomorphic adenomas and Warthin tumors. ** = *P* value for comparison of pleomorphic adenomas and malignant tumors. The T_{peak} for the pleomorphic adenomas was significantly longer than those for the Warthin ($P < .0001$) and malignant ($P < .001$) tumors.

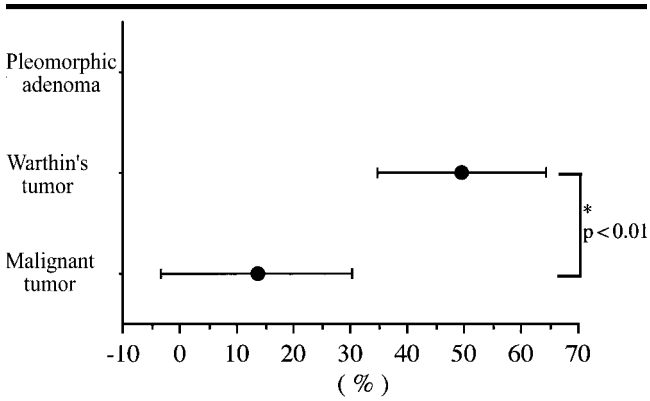

Figure 3. Plotted WR values. The dots represent means, and the lines through the dots represent SDs. The WR data for pleomorphic adenomas were not applicable, because nine of the 12 pleomorphic adenomas showed gradual enhancement and one showed a flat TIC. * = *P* value indicates that the WR for Warthin tumors was significantly higher than that for the malignant tumors.

TABLE 2
Performance Values of T_{peak} for Differentiation of Benign from Malignant Tumors

	T_{peak}		
Performance Value	90 sec	120 sec	150 sec
Sensitivity	6/9 (67)	9/9 (100)	9/9 (100)
Specificity	10/18 (56)	9/18 (50)	8/18 (44)
Positive predictive value	6/14 (43)	9/18 (50)	9/19 (47)
Negative predictive value	10/13 (77)	9/9 (100)	8/8 (100)
Accuracy	16/27 (59)	18/27 (67)	17/27 (63)

Note.—Data are numbers of patients. Numbers in parentheses are percentages. Two cases in which there was marked cystic change were excluded because the ROI could not be plotted. A T_{peak} of 120 seconds was chosen as the cutoff value for distinguishing malignant from benign tumors because it had the highest accuracy.

TABLE 3
Performance Values of WR for Differentiation of Benign from Malignant Tumors

	WR				
Performance Value	20%	25%	30%	35%	40%
Sensitivity	6/9 (67)	7/9 (78)	8/9 (89)	8/9 (89)	8/9 (89)
Specificity	8/9 (89)	7/9 (78)	7/9 (78)	5/9 (56)	4/9 (44)
Positive predictive value	6/7 (86)	7/9 (78)	8/10 (80)	8/12 (67)	8/13 (62)
Negative predictive value	8/11 (73)	7/9 (78)	7/8 (88)	5/6 (83)	4/5 (80)
Accuracy	14/18 (78)	14/18 (78)	15/18 (83)	13/18 (72)	12/18 (67)

Note.—Data are numbers of patients. Numbers in parentheses are percentages. Nine cases in which there was a gradual enhancement pattern and two cases in which there was marked cystic change were excluded. A WR of 30% was chosen as the cutoff value for distinguishing malignant from benign tumors because it had the highest accuracy.

lesions (in 20 patients) was 25.2 mm, and that of the malignant tumors (in nine patients) was 27.4 mm. According to *t* test results, there was no statistically significant difference in maximum tumor diameter between the benign and malignant tumors ($P = .59$).

MR Imaging

A 0.5-T MR imaging unit (Vectra EX; GE-Yokogawa Medical Systems, Tokyo, Japan) was used. Pre- and postcontrast transverse T1-weighted spin-echo (repetition time msec/echo time msec, 400/20) and transverse T2-weighted fast spin-echo (2,200/100) MR images were obtained in all cases. A 20-cm field of view, a 5-mm-thick section at 6-mm intervals, and a 256 × 128 matrix with two signals acquired were used. In all patients, tumors were identified on the transverse T1-weighted MR images, and the section that included the maximum diameter of the tumor was selected for dynamic imaging. When there were two or three tumors in the same salivary gland, an oblique MR image was used for the dynamic study so that all tumors would be included.

Dynamic MR imaging was performed by using a single-section technique with a spin-echo pulse sequence (150/16). A 20-cm field of view, a 7-mm-thick section, and a 256 × 160 matrix with one signal acquired were used. Gadopentetate dimeglumine (0.2 mL per kilogram of body weight) was administered intravenously. MR images were sequentially obtained before and 30, 60, 90, 120, 150, 180, 240, and 300 seconds after contrast material administration. One author (H.Y.) manually drew regions of interest for signal intensity measurement to avoid the vessels and cystic parts of the tumors. The region of interest was never smaller than 0.1 cm^2 and was approximately 3–4 mm in diameter in most cases. When the contrast enhancement was heterogeneous, the signal intensities of multiple areas were measured and the area with maximal enhancement was selected. Thereafter, TICs were constructed.

The parameters derived from the TICs were SI_{peak}, which was defined as the first signal intensity (SI) measurement that

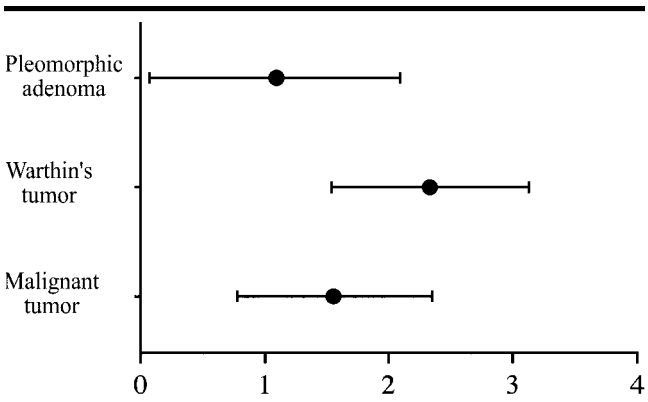

Figure 4. Plotted slope values. The dots represent means, and the lines through the dots represent SDs. There was no statistically significant difference in slope among the histopathologic tumor subtypes.

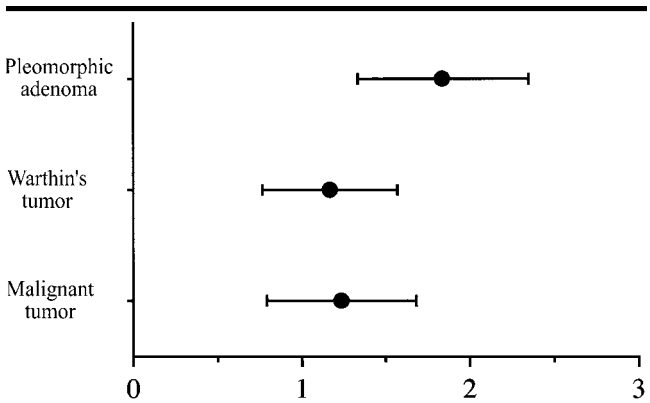

Figure 5. Plotted ER values. The dots represent means, and the lines through the dots represent SDs. There was no statistically significant difference in ER among the histopathologic tumor subtypes.

satisfied the inequality SI > [0.9(SI_{max} − SI_{pre})] + SI_{pre}, and T_{peak}, which was the time that corresponded to the SI_{peak}. SI_{pre} was the precontrast signal intensity, and SI_{max} was the signal intensity at maximal contrast enhancement. We did not define T_{peak} as the time that corresponded to the SI_{max}, as was done in earlier studies (16–18). When we have defined T_{peak} as the time that corresponded to the SI_{max}, we have found it difficult to determine a reliable T_{peak} in cases in which the TIC showed an early peak and plateau enhancement pattern, because signal intensity can change to a very small degree within an error during the plateau phase. Enhancement ratio (ER) was defined as follows: (SI_{max} − SI_{pre})/SI_{pre}. Slope was defined as [(SI_{peak} − SI_{pre})/(SI_{pre} × T_{peak})] × 100 and expressed as a percentage per second, as was done by Buadu et al (18), because absolute signal intensity measurements can vary according to the capability and settings of the MR unit. Washout ratio (WR), expressed as a percentage, was defined as follows: [(SI_{max} − SI_{5min})/(SI_{max} − SI_{pre})] × 100 (%), where SI_{5min} is the signal intensity at 5 minutes after contrast material administration. We used SI_{peak} instead of SI_{max} to calculate the slope as the same reason when we defined SI_{peak}. The parameters of TIC are summarized in Figure 1.

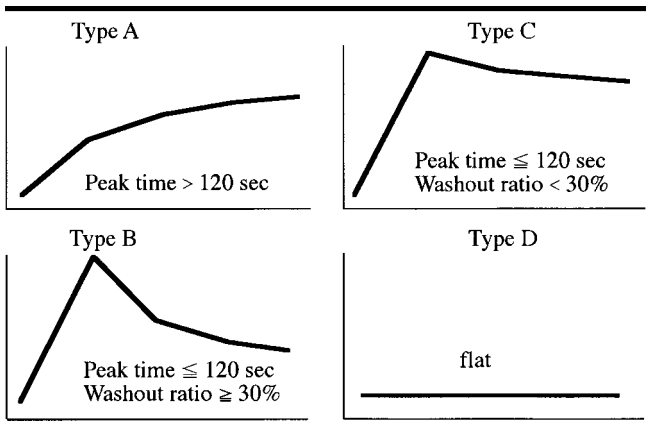

Figure 6. TIC tumor type classifications.

Histopathologic Analysis

One pathologist (Y.H.) examined all of the histopathologic specimens without knowledge of the MR imaging findings. Histopathologic specimens stained with hematoxylin-eosin were examined to determine the degree of cellularity and stromal reaction, which was graded by using a scale of 1 (noncellular) to 4 (highly cellular). Immunohistochemical analysis with anti-CD34 stain was performed by using the avidin-biotin-peroxidase complex to determine the vascularity of the tumors. The vessels were counted by using the technique described by Buadu et al (18). Any brown-stained endothelial cell or cluster of cells that was clearly distinct from adjacent tumor cells and connective tissue elements was considered to be a single countable microvessel.

The area of the highest neovascularity was identified at low power (×40 and ×100) with a model BX50 microscope (Olympus, Tokyo, Japan). The microvessel count was obtained by averaging the number of microvessels at five points in this area in a ×200 magnification field (ie, ×20 objective lens and ×10 ocular lens) in each salivary gland tumor. The histopathologic characteristics of each type of salivary gland tumor also were analyzed.

Statistical Analysis

In this study, all statistical analyses were performed by using nonparametric statistical tests because we could not assume a normal distribution of the interval variables or the categorical nature of the cellularity-stromal grade. In addition, at analysis of the TIC parameters, we performed a per-person rather than per-tumor analysis to avoid a lack of independence, because our study included two mucoepidermoid carcinomas in one patient, two acinic cell carcinomas in one patient, and three Warthin tumors in one patient. Statistical analyses with the Spearman rank correlation coefficient were performed to determine the strengths of correlations between T_{peak} and microvessel count and between WR and cellularity-stromal grade. Statistical analysis was also performed to determine whether any differences related to TIC parameters—namely, T_{peak}, slope, ER, and WR—could

TABLE 4
TIC Types among Various Histopathologic Diagnoses

Diagnosis	TIC Type*			
	A	B	C	D
	Initial Study			
Benign				
Pleomorphic adenoma (n = 12)	9	0	2	1
Warthin tumor (n = 9)	0	8	0	1
Myoepithelioma (n = 1)	0	1	0	0
Malignant				
Carcinoma (n = 9)	0	0	9	0
Non-Hodgkin lymphoma (n = 2)	0	1	1	0
	Validation Study			
Benign				
Pleomorphic adenoma (n = 5)	3	0	1	1
Warthin tumor (n = 4)	0	4	0	0
Eosinophilic granuloma (n = 1)	0	0	1	0
Malignant				
Carcinoma (n = 3)	0	0	3	0

* Data are numbers of tumors. Type A = $T_{peak} > 120$ seconds; type B = $T_{peak} \leq 120$ seconds, WR $\geq$ 30%; type C = $T_{peak} \leq 120$ seconds, WR $<$ 30%; type D = flat TIC.

TABLE 5
Diagnostic Effectiveness of TIC Types in Identification of Malignant Tumors among Benign and Malignant Salivary Gland Tumors

Study	Sensitivity	Specificity	Accuracy	PPV	NPV
Initial	10/11 (91)	20/22 (91)	30/33 (91)	10/12 (83)	20/21 (95)
Validation	3/3 (100)	8/10 (80)	11/13 (85)	3/5 (60)	8/8 (100)

Note.—Data are numbers of tumors. Numbers in parentheses are percentages. NPV = negative predictive value, PPV = positive predictive value.

be observed among the histopathologic types. The Kruskal-Wallis test was performed to determine whether any differences among the various histopathologic types could be seen. If Kruskal-Wallis test results were positive, we also applied Bonferroni correction to determine whether any differences between two specific histopathologic types existed. All statistical analyses were performed with a computer software statistics program (Statview 5.0 for Macintosh; SAS Institute, Cary, NC).

Validation Study

The described statistical analyses were not performed in a completely prospective manner, because MR imaging data analysis was performed either before or after the histopathologic studies of the resected specimens. To test the true diagnostic value of four TIC tumor types that were classified on the basis of a T_{peak} of 120 seconds and a WR of 30%, we prospectively examined 13 salivary gland tumors in 13 consecutive patients at dynamic gadolinium-enhanced MR imaging between July 2000 and June 2001. In type A, the T_{peak} was longer than 120 seconds. A salivary gland tumor of this type was considered to have gradual enhancement. In type B, the T_{peak} was shorter than or equal to 120 seconds and the WR was greater than or equal to 30%. A salivary gland tumor of this type was considered to have early enhancement and high washout. In type C, T_{peak} was shorter than or equal to 120 seconds and the WR was less than 30%. A salivary gland tumor with this pattern was considered to have early enhancement and low washout. In type D, the TIC was flat. A salivary gland tumor of this type was considered to be markedly cystic. The TIC type of each salivary gland tumor was determined before surgery in all patients. The technique used to image and evaluate the tumors was otherwise the same as that used in the initial part of the study.

Five pleomorphic adenomas, four Warthin tumors, two adenoid cystic carcinomas, one adenocarcinoma, and one eosinophilic granuloma were analyzed in the validation study. We examined the sensitivity, specificity, positive predictive value, negative predictive value, and accuracy of the TIC tumor classifications in the differentiation of malignant from benign tumors when malignancy was considered a positive result.

RESULTS

MR Image Evaluation

Figure 2 shows the distribution of T_{peak} values. All tumors with a T_{peak} longer than 120 seconds were benign, and tumors with a T_{peak} shorter than 120 seconds were either benign or malignant. To find a reasonable threshold to distinguish malignant from benign lesions, we compared the sensitivity, specificity, accuracy, and predictive values of T_{peak} values of 90, 120, and 150 seconds when malignancy was considered a positive result. We chose 120 seconds as the cutoff T_{peak} to maximize accuracy (Table 2). Figure 3 shows the distribution of WRs. To find a reasonable threshold to distinguish malignant from benign lesions, we compared the sensitivity, specificity, accuracy, and predictive values of WRs of 20%, 25%, 30%, 35%, and 40% when malignancy was considered a positive result. We chose 30% as the cutoff WR on the basis of the high accuracy measure (Table 3). The slopes and ERs for various histopathologic tumor types are illustrated in Figures 4 and 5, respectively. There was no statistically significant difference in slope or ER between the benign and malignant tumors.

Statistically significant differences in T_{peak} and WR were seen among the histopathologic tumor types at Kruskal-Wallis analysis. At T_{peak} analysis with Bonferroni correction, significant differences between pleomorphic adenomas and Warthin tumors ($P <$ .0001) and between pleomorphic adenomas and malignant tumors ($P <$ .001) were seen. At WR analysis with Bonferroni correction, there was a significant difference between Warthin and malignant tumors ($P <$ .01). On the basis of these results, we categorized the salivary gland tumors into the four TIC types according to a T_{peak} of 120 seconds and a WR of 30% (Fig 6). There were nine type A, 10 type B, 12 type C, and two type D tumors in the initial part of our study.

Table 4 shows the distributions of benign and malignant tumors among the four TIC tumor types. Of the 12 pleomorphic adenomas, nine (75%) were type A

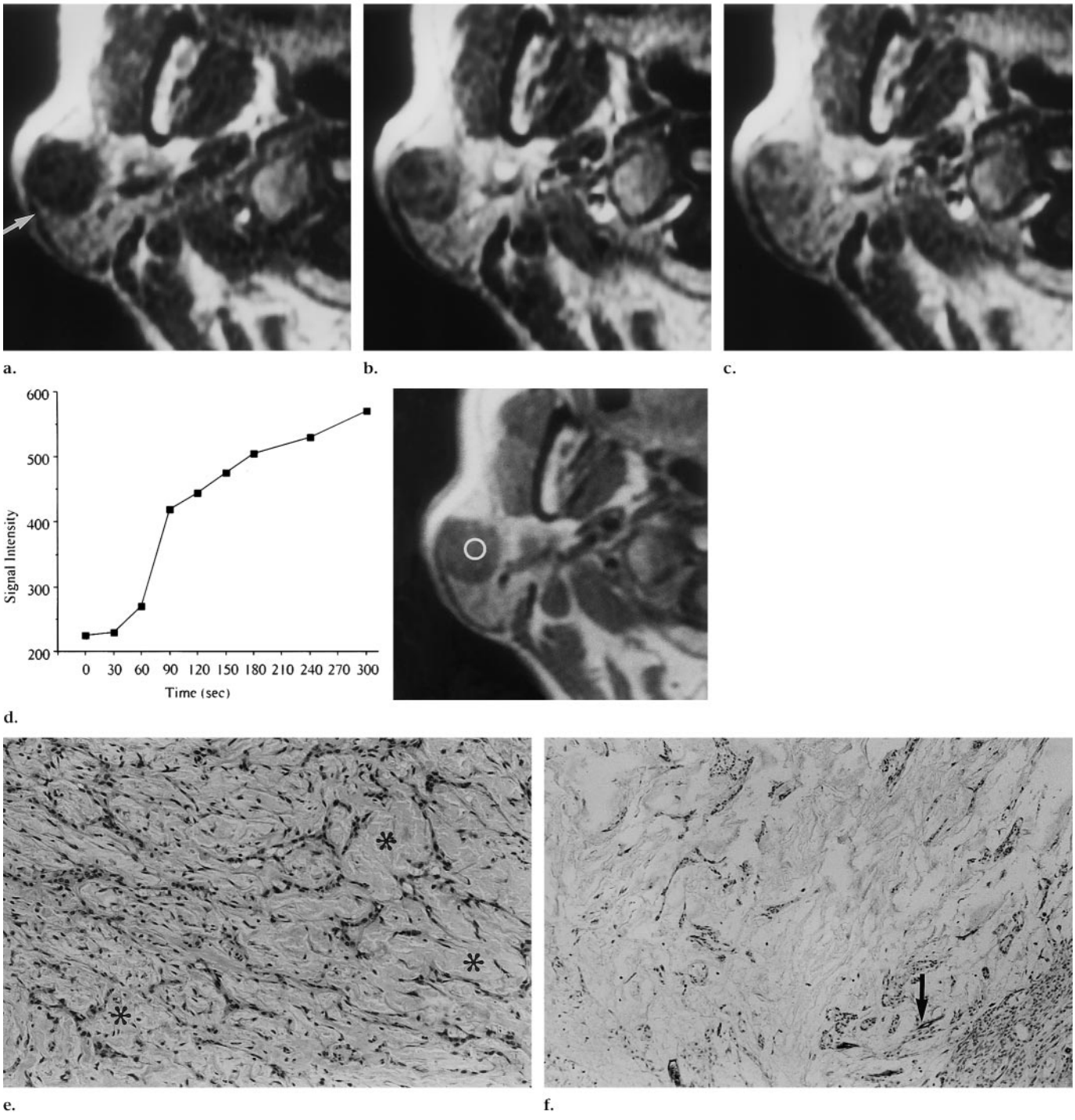

Figure 7. Pleomorphic adenoma of the right parotid gland in a 70-year-old man. **(a)** Transverse T1-weighted spin-echo MR image (400/20) shows a well-defined hypointense mass (arrow) in the right parotid gland. **(b)** Transverse T1-weighted spin-echo MR image (150/16) obtained 90 seconds after contrast material administration shows moderate tumor enhancement. **(c)** Transverse T1-weighted spin-echo MR image (150/16) obtained 300 seconds after contrast material administration shows gradual tumor enhancement. **(d)** TIC (left) and corresponding transverse T1-weighted spin-echo MR image (150/16) (right) depict the gradual enhancement pattern (type A). The T_{peak} is 180 seconds. Right: The round cursor marks the region of interest selected for signal intensity measurement at dynamic MR imaging. **(e)** Microscopic view of the adenoma specimen shows minimal epithelial elements and an abundant myxoid matrix (*); the cellularity-stromal grade is 1 (acellular). (Hematoxylin-eosin stain; original magnification, ×40.) **(f)** Immunohistochemically stained microscopic section shows a scarcity of microvessels (arrow); the microvessel count is 3.6. (Anti-CD34 stain; original magnification, ×200.)

tumors (Fig 7a–7d), two were type C tumors, and one was a type D tumor. Eight of the nine Warthin tumors were type B neoplasms (Fig 8a), but one was a type D neoplasm. All of the malignant tumors, except one lymphoma, were type C neo-

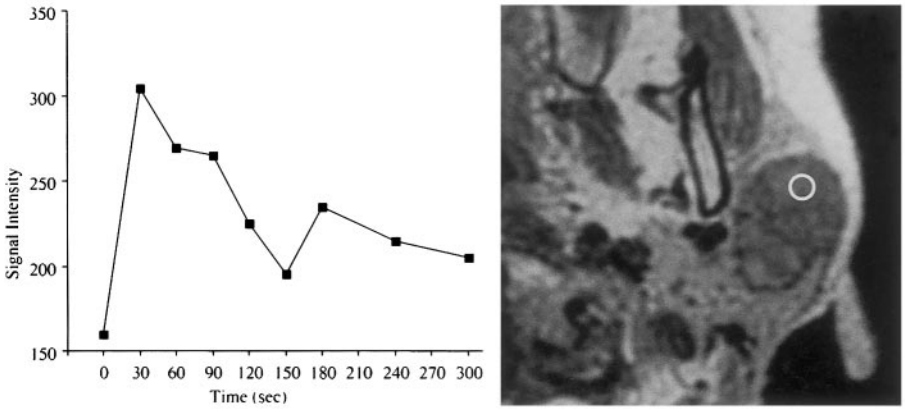

a.

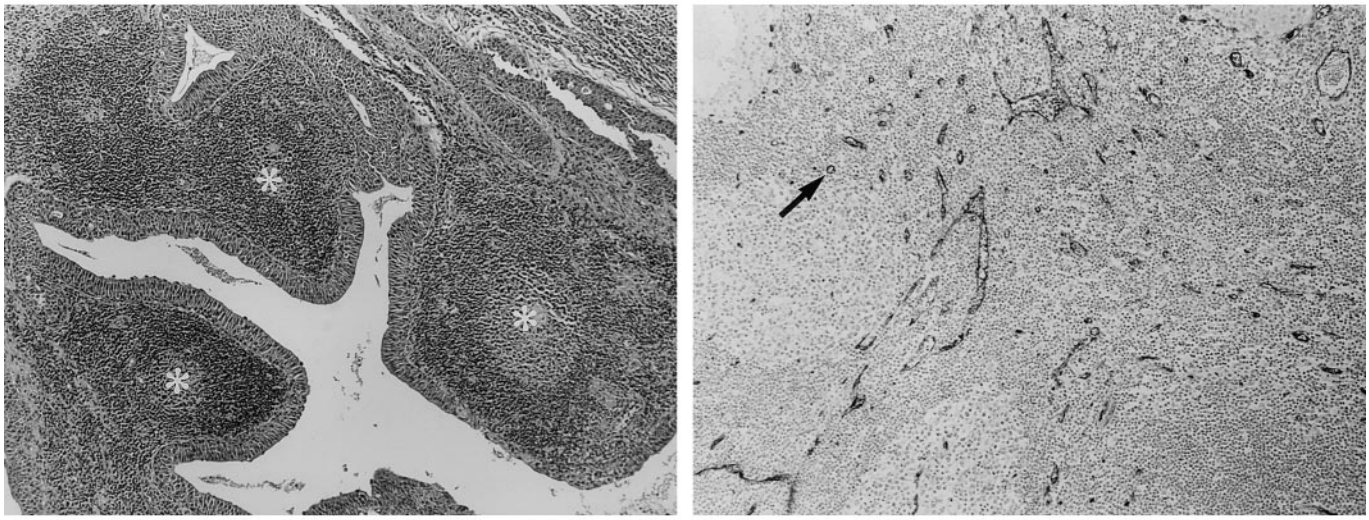

b. c.

Figure 8. Warthin tumor of the left parotid gland in a 74-year-old woman. **(a)** TIC (left) and corresponding transverse T1-weighted spin-echo MR image (150/16) (right) depict an early peak of enhancement and a high washout pattern (type B). The T_{peak} is 30 seconds, and the WR is 71%. Right: The round cursor marks the region of interest selected for signal intensity measurement at dynamic MR imaging. **(b)** Microscopic view of the tumor specimen shows a proliferation of eosinophilic cells in the cyst wall and lymph follicle formation (*); the cellularity-stromal grade is 4 (highly cellular). (Hematoxylin-eosin stain; original magnification, ×40.) **(c)** Immunohistochemically stained section shows abundant microvessels (arrow); the microvessel count is 60. (Anti-CD34 stain; original magnification, ×200.)

plasms (Fig 9a). In the initial part of our study, when we regarded type A, B, and D tumors as benign neoplasms and type C tumors as malignant neoplasms, the sensitivity, specificity, accuracy, positive predictive value, and negative predictive value of TIC-based tumor differentiation were 91% (10 of 11 tumors), 91% (20 of 22 tumors), 91% (30 of 33 tumors), 83% (10 of 12 tumors), and 95% (20 of 21 tumors), respectively (Table 5).

Histopathologic Analysis

The graph in Figure 10 illustrates the correlation between T_{peak} and microvessel count. The correlation between T_{peak} and microvessel count was significantly different from zero ($P < .0001$, $\rho = -0.800$). The graph in Figure 11 illustrates the correlation between WR and cellularity-stromal grade. The correlation between WR and cellularity-stromal grade was significantly different from zero ($P = .0105$, $\rho = 0.572$). No statistically significant correlation between ER and histopathologic findings or between slope and histopathologic findings was seen.

Of the 12 pleomorphic adenomas, nine (75%) had a histopathologically abundant myxoid matrix and scarce epithelial components, a low microvessel count, and a low cellularity-stromal grade (Fig 7e, 7f). The two type C pleomorphic adenomas had histopathologically abundant epithelial elements with a small amount of myxoid matrix, and the type D pleomorphic adenoma had markedly cystic changes. Of the nine Warthin tumors, eight showed abundant small (ie, capillary-sized) vessels and high cellularity (Fig 8b, 8c) at histopathologic analysis; the type D neoplasm showed markedly cystic changes. Nine (82%) of the 11 malignant tumors had a high microvessel count and a low cellularity-stromal grade. Abundant fibrous stromata existed in all nine carcinomas (Fig 9b, 9c), but the two malignant lymphomas had an almost purely cellular pattern and scarce stromata.

Validation Study Results

Tables 1, 4, and 5 also show the results of the validation study involving 13 tumors in 13 patients. All three type A tumors were pleomorphic adenomas, and all four type B tumors were Warthin tumors. Of the five type C tumors, two were adenoid cystic carcinomas,

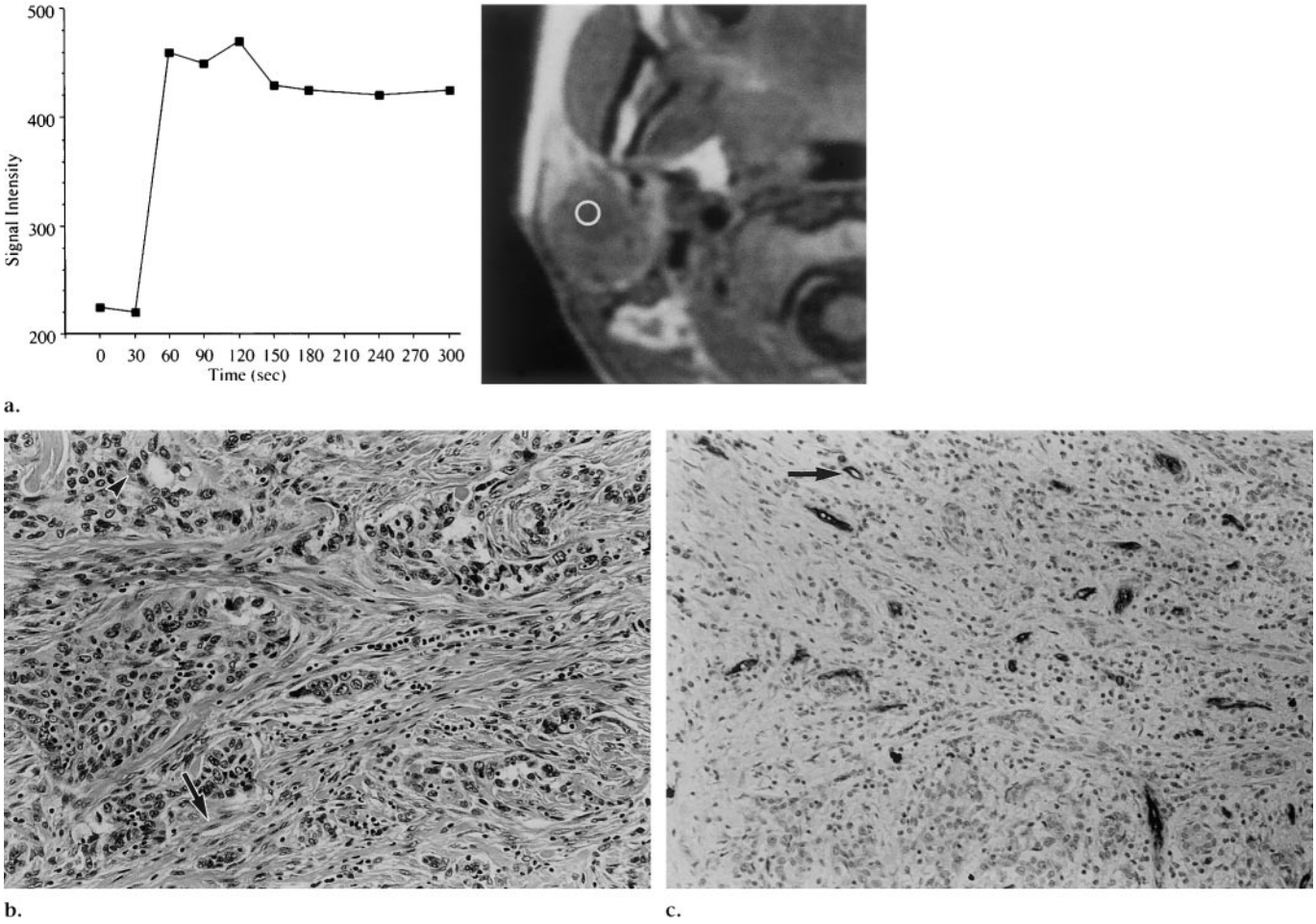

Figure 9. High-grade mucoepidermoid carcinoma of the right parotid gland in a 70-year-old man. **(a)** TIC (left) and corresponding transverse T1-weighted spin-echo MR image (150/16) (right) depict an early peak of enhancement and a low washout pattern (type C). The T_{peak} is 60 seconds, and the WR is 21%. Right: The round cursor marks the region of interest selected for signal intensity measurement at dynamic MR imaging. **(b)** Microscopic view of the carcinoma specimen shows a proliferation of spindle-shaped cells (arrow) with a high nucleus-cytoplasm ratio. An abundance of fibrous stromal tissue and a glandular formation (arrowhead) also are seen. The cellularity-stromal grade is 2. (Hematoxylin-eosin stain; original magnification, ×40.) **(c)** Immunohistochemically stained section shows abundant microvessels (arrow); the microvessel count is 23. (Anti-CD34 stain; original magnification, ×200.)

one was an adenocarcinoma, one was a pleomorphic adenoma, and one was an eosinophilic granuloma. The one type D tumor was a pleomorphic adenoma. When we regarded type A, B, and D tumors as benign neoplasms and type C tumors as malignant neoplasms, the sensitivity, specificity, accuracy, positive predictive value, and negative predictive value were 100% (three of three tumors), 80% (eight of 10 tumors), 85% (11 of 13 tumors), 60% (three of five tumors), and 100% (eight of eight tumors), respectively (Table 5).

DISCUSSION

The surgery chosen for treatment of salivary gland tumors depends on the location and histologic type of the tumor (1–4). When the tumor is malignant, total parotidectomy or lobectomy is selected and the facial nerve may be sacrificed (2,3). Therefore, preoperative differentiation between benign and malignant tumors is very important with regard to obtaining informed consent, which may involve documenting the patient's willingness to be placed at risk for postsurgical complications such as facial nerve palsy. The results of preoperative aspiration cytology are sometimes inconclusive or false, however, owing to insufficient specimen samples, small tumor size, or a problematic tumor location—for example, the deep lobe of the parotid gland and the parapharyngeal space (5–7). Thus, the ability to predict the existence of benign or malignant tumors on the basis of imaging findings would be very useful with regard to obtaining informed consent preoperatively.

There have been reports of MR imaging findings of salivary gland tumors (8–15). The static MR imaging characteristics of malignant salivary gland tumors reportedly are irregular tumor margin, signal intensity heterogeneity, tumor infiltration into surrounding tissue, and low signal intensity on T2-weighted images (8,9). Som and Biller (8) observed that high-grade malignancies of the parotid gland usually had poorly defined margins and low signal intensity on both T1- and T2-weighted MR images. Swartz et al (9) reported that tumor homogeneity and signal intensity correlated well with

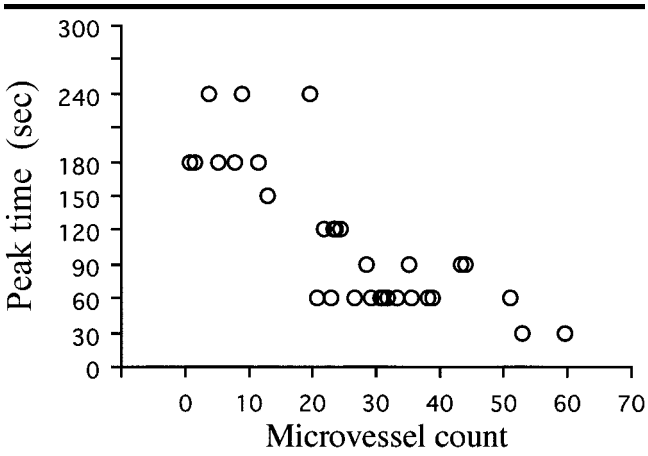

Figure 10. Graph illustrates the correlation between T_{peak} and microvessel count. The correlation was significantly different from zero ($P < .0001$, $\rho = -0.800$).

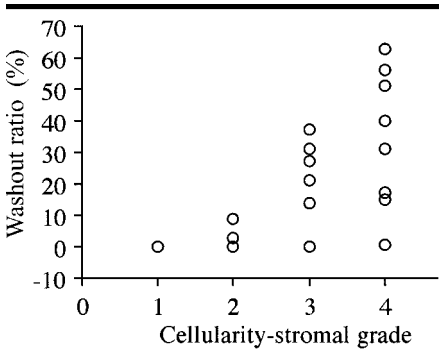

Figure 11. Graph illustrates the correlation between WR and cellularity-stromal grade. The correlation was significantly different from zero ($P = .0105$, $\rho = 0.572$).

histologic findings. On the other hand, Teresi et al (10) reported that tumor homogeneity was not a useful criterion for distinguishing benign from malignant disease.

Freling et al (11) observed tumor infiltration into deep structures (eg, the parapharyngeal space, muscles, and bone) only with malignant tumors; other MR imaging factors, such as tumor margin, homogeneity, and signal intensity, were not useful for differentiating between benign and malignant disease. Joe and Westesson (12) reported that infiltration into muscles was the only finding that was suggestive of malignant tumors. Thus, the role of static MR imaging in the differentiation of benign and malignant salivary gland tumors appears to be controversial.

With regard to dynamic MR imaging, Takashima et al (16) reported the results of performing this examination to image the head and neck. They examined 49 salivary gland lesions by using dynamic MR imaging and assigned the lesions to five groups according to TIC peaks: Type A lesions showed peak enhancement 0–30 seconds after contrast material administration; type B, at 30–60 seconds; and type C, at 60–210 seconds. Type D lesions had a gradual slope of enhancement, and type E lesions showed a flat curve. These authors classified tumors according to T_{peak} only, and their definition of T_{peak} differed from that used in our study (defined in Materials and Methods). According to their results, only four of 21 pleomorphic adenomas showed an early enhancement peak, at fewer than 60 seconds after contrast material administration; eight of 10 Warthin tumors showed a peak at fewer than 60 seconds; and five of 11 malignant tumors showed gradual enhancement.

Our study results appear to be consistent with those of Takashima et al (16) in terms of the long T_{peak} for pleomorphic adenomas and the short T_{peak} for Warthin tumors but different from their results in terms of the T_{peak} values for malignant tumors. The tumors with a type C TIC pattern in our study could be categorized as having a gradual enhancement pattern according to the definitions used by Takashima et al. In their study, 11 malignant tumors showed type B, C, or D enhancement patterns, but 27 (71%) of 38 benign lesions also had the same patterns. They concluded that dynamic MR imaging contributes little to the prediction of malignancy but can help narrow the differential diagnosis and is potentially useful in determining tumor vascularity.

Tsushima et al (17) examined 18 parotid and five parapharyngeal tumors by using dynamic MR imaging. According to their results, seven pleomorphic adenomas and two adenoid cystic carcinomas showed gradual enhancement during the first 260 seconds after contrast material administration, seven Warthin tumors showed rapid enhancement during the first 20 seconds and then a decrease in signal intensity, and the other malignant tumors showed a rapid increase in signal intensity during the first 20 seconds and then a gradual decrease or increase in signal intensity. They concluded that dynamic MR imaging could help distinguish pleomorphic adenoma from Warthin tumor but not pleomorphic adenoma from adenoid cystic carcinoma or Warthin tumor from other malignant tumors. The Takashima et al (16) and Tsushima et al (17) reports both focused on the T_{peak} for salivary gland tumors.

In the present study, we analyzed other TIC parameters as well as the T_{peak} and correlated these parameters with histopathologic findings. According to the results of our study, T_{peak} correlated closely with microvessel count and the WR accurately reflected the cellularity-stromal grade. The microvessel count is considered to represent tumor vascularity, and the T_{peak} will be short if the microvessel count is high. The WR depends on the difference in the amount of contrast material within the tumor between the intravascular and extravascular phases. A large extracellular space with fibrous stromata reportedly retains contrast material for a certain period (19). Therefore, tumors with a high cellularity-stromal grade will retain less contrast material and have a high WR, whereas those with a low cellularity-stromal grade will have a low WR.

ER correlated with neither tumor vascularity nor cellularity-stromal grade. We speculate that even when tumor vascularity is low, the ER can be high if there is a large amount of stromata that continue to accumulate contrast material. The slope of enhancement can be affected by both ER and T_{peak}, because the slope is approximately equal to ER/T_{peak}. Therefore, we speculate that ER and slope do not have a statistically significant correlation when the relationship is analyzed according to histopathologic findings and/or tumor types.

The long T_{peak} for pleomorphic adenoma is consistent with a low microvessel count and low cellularity-stromal grade. However, two epithelial-dominant pleomorphic adenomas with high microvessel counts and low cellularity-stro-

mal grades could not be discriminated from malignant tumors on the basis of TIC type. The short T_{peak} and high WR for Warthin tumors can be explained by their high microvessel count and high cellularity-stromal grade. The short T_{peak} and low WR for malignant tumors can be explained by their high microvessel count and low cellularity-stromal grade. We speculate that the tumor angiogenesis and abundant fibrous stromata in nine carcinomas, out of 11 malignant tumors, could be attributed to a high microvessel count and a low cellularity-stromal grade, respectively. The TIC patterns of two malignant lymphomas were different from those of the carcinomas: One lymphoma was a type B tumor, and the other was a type C tumor. However, we could not detect a histopathologic difference between these two cancers.

According to our study results, a T_{peak} of 120 seconds enabled the differentiation of pleomorphic adenomas from malignant tumors, although assessment of the T_{peak} alone did not enable differentiation of Warthin tumors from malignant tumors. The WRs for Warthin tumors were significantly higher than those for the malignant tumors. Therefore, the combined assessment of T_{peak} and WR enabled the differentiation of pleomorphic adenomas, Warthin tumors, and malignant tumors, and TIC types classified according to T_{peak} and WR had high sensitivity and specificity in the differentiation of benign and malignant tumors. The results of our validation study also proved that the described criteria can facilitate predictions of whether a salivary gland tumor is benign or malignant.

In the initial study, two type D tumors included one pleomorphic adenoma and one Warthin tumor. Cystic changes are more commonly seen in Warthin tumors, but they can also be seen in pleomorphic adenomas and malignant tumors (13). Markedly cystic changes, with which a region of interest larger than 0.1 cm^2 cannot be plotted in the solid portion of a tumor, were not seen in the malignant tumors in our study. We speculate that there were some residual solid portions because cystic changes in malignant tumors, as opposed to tumors that are almost entirely cystic in nature, are considered to be secondary to necrosis.

This study had some limitations. First, a small number of malignant tumors were included in this study. Second, we examined only the central portion of the tumors because the MR unit used in this study did not have multisection dynamic imaging capability. Those tumors that contained diverse elements of epithelial-dominant or stromal-dominant portions, such as pleomorphic adenoma, mucoepidermoid carcinoma, and adenoid cystic carcinoma, might show different TIC patterns depending on the section selected. Finally, the examiner selected the location of the region of interest.

In conclusion, the T_{peak} and WR derived from TICs at gadolinium-enhanced dynamic MR imaging correlate well with histopathologic findings. A long T_{peak} for pleomorphic adenomas, a short T_{peak} and high WR for Warthin tumors, and a short T_{peak} and low WR for malignant tumors were observed in most instances. Four TIC types that are classified on the basis of a T_{peak} of 120 seconds and a WR of 30% are useful in predicting whether salivary gland tumors are benign or malignant.

References

1. Yu GY, Ma DQ, Liu XB, et al. Local excision of the parotid gland in the treatment of Warthin's tumour. Br J Oral Maxillofac Surg 1998; 36:186–189.
2. Carlson GW. The salivary glands. Embryology, anatomy, and surgical applications. Surg Clin North Am 2000; 80:261–273.
3. Magnano M, Gervasio CF, Cravero L, et al. Treatment of malignant neoplasms of the parotid gland. Otolaryngol Head Neck Surg 1999; 121:627–632.
4. Rehberg E, Schroeder HG, Kleinsasser O. Surgery in benign parotid tumors: individually adapted or standardized radical interventions? Laryngorhinootologie 1998; 77:283–288. [German]
5. Layfield LJ, Tan P, Glasgow BJ. Fine-needle aspiration of salivary gland lesions: comparison with frozen sections and histologic findings. Arch Pathol Lab Med 1987; 111:346–353.
6. Zurrida S, Alasio L, Tradati N, et al. Fine-needle aspiration of parotid masses. Cancer 1993; 72:2306–2311.
7. Takashima S, Takayama F, Wang Q, Kurozumi M, Sekiyama Y, Sone S. Parotid gland lesions: diagnosis of malignancy with MRI and flow cytometric DNA analysis and cytology in fine-needle aspiration biopsy. Head Neck 1999; 21: 43–51.
8. Som PM, Biller HF. High-grade malignancies of the parotid gland: identification with MR imaging. Radiology 1989; 173: 823–826.
9. Swartz JD, Rothman MI, Marlowe FI, et al. MR imaging of parotid mass lesions: attempts at histopathologic differentiation. J Comput Assist Tomogr 1989; 13:789–796.
10. Teresi LM, Lufkin RB, Wartham DG, Abemayor E, Hanafee WN. Parotid masses: MR imaging. Radiology 1987; 163:405–409.
11. Freling NJ, Molenaar WM, Vermey A, et al. Malignant parotid tumors: clinical use of MR imaging and histologic correlation. Radiology 1992; 185:691–696.
12. Joe VQ, Westesson PL. Tumors of the parotid gland: MR imaging characteristics of various histologic types. AJR Am J Roentgenol 1994; 163:433–438.
13. Minami M, Tanioka H, Oyama K, et al. Warthin tumor of the parotid gland: MR-pathologic correlation. AJNR Am J Neuroradiol 1993; 14:209–214.
14. Mascaro L, Ferrari C, Grazioli L, et al. T2 relaxation of the parotid gland of patients affected by pleomorphic adenoma. Magn Reson Imaging 1999; 17:723–730.
15. Yousem D, Kraut MA, Chalian AA. Major salivary gland imaging. Radiology 2000; 216:19–29.
16. Takashima S, Noguchi Y, Okumura T, et al. Dynamic MR imaging in the head and neck. Radiology 1993; 189:813–821.
17. Tsushima Y, Matsumoto M, Endo K. Parotid and parapharyngeal tumours: tissue characterization with dynamic magnetic resonance imaging. Br J Radiol 1994; 67: 342–345.
18. Buadu LD, Murakami J, Murayama S, et al. Breast lesions: correlation of contrast medium enhancement patterns on MR images with histopathological findings and tumor angiogenesis. Radiology 1996; 200:639–649.
19. Murakami T, Nakamura H, Tsuda K, et al. Contrast-enhanced MR imaging of intrahepatic cholangioma: pathologic correlation study. J Magn Reson Imaging 1995; 5:165–170.